# 8

# High Performance Data-Driven Multiscale Inverse Constitutive Characterization of Composites

In this chapter, we present recent advances in the multi-scale data-driven inverse constitutive characterization of composites via multi-axial robotic testing, high-performance full-field strain measurement methods and surrogate models. Emphasis is given first on the motivating aspects for multi-scale model inversion for the case of laminated composites, followed by a description of a data-driven inverse constitutive characterization of the bulk lamina of composites via multi-axial loading of laminate-level coupons. A description of a surrogate modeling approach is presented in order to address the computational cost involved in the forward model evaluations associated with the optimization required for material characterization. Finally, we present progress in identifying material properties at the lower scales by utilizing experiments in the laminate-level macro-scale.

Chapter written by John MICHOPOULOS, Athanasios ILIOPOULOS, John HERMANSON, John STEUBEN and Foteini KOMNINELI.

## 8.1. Introduction

Our main long-term goal is to establish a computational infrastructure that can relate performance and usability specifications of material systems to their optimized manufacturing by design. As described in [MIC 10b], to achieve this goal it is essential to establish the ability to perform inverse analysis on multi-scale cascaded model chains, bridging the macro-scale with the micro- and nano-scales. This is predicated by the fact that behavioral data can be collected more easily in the macro-scale and that manufacturing process parameters (e.g. precursor constituents composition and pressure and temperature of monomer autoclaves) affect the thermo-mechanical properties of these material systems at the micro length scales, as shown elsewhere [FU 16]. That is, in order to achieve desired functional outcomes at the macro-scale by controlling the process parameters in the lower length scales, it is necessary to connect the various models that can be built and linked across the relevant scales. This process is depicted in Figure 8.1. Specifically, instead of determining the proper process parameters from the functional specification of the material system to be developed through direct inversion of a single model (as shown in the top path of Figure 8.1), we envision the inversion of a cascade of models distributed along various scales through the lower path of the figure.

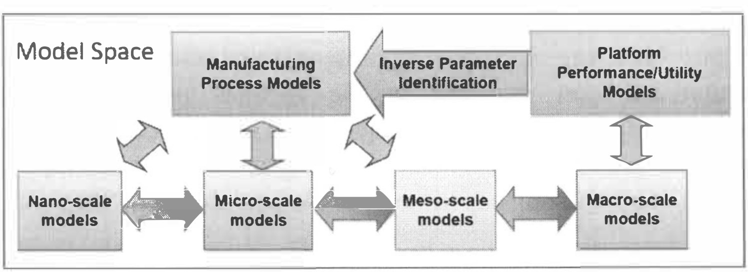


**Figure 8.1.** *Computational framework depicting equivalency of inverse problems connecting macro-scale functional specification with process parameters with inverse problem of cascaded chain of models along multiple length scales*

Our main short-term goal is to demonstrate that such a framework can be useful for designing a material system relevant to a wide variety of applications. A material system that is suitable to demonstrate at least a three-level length-scale cascade is that of the polymer matrix fiber composites (PMFCs). At the micro-scale, the constituents of the composite, namely the fibers and the matrix, appear as individual deformable continua with distinctly different properties. At the meso-scale, the thin individual lamina (or ply) can be abstracted as a homogenized transversely isotropic material sub-system with a major axis of orthotropy along the direction of the fibers. At the macro-scale, stacks of laminae form the composite material laminates that in general appear as anisotropic materials, but in some cases can appear as orthotropic or even transversely isotropic materials depending on the stacking sequence.

In order to achieve these goals, and because mechanical testing can occur easily at the macro-scale, we have decided to examine the potential of solving the composition of the structural equilibrium equations at each scale in such a manner that instead of determining the linear anisotropic elastic parameters of the laminate at the macro-scale level as an effective material, we determine the properties of the individual constituents at the micro-scale. This has a particularly important utility especially if we consider that some of the anisotropic moduli of the fibers cannot always be determined experimentally.

In addition, we are motivated by a specific variation of our long-term goal to be able to assess performance specification requirements that sometimes involve quantification of material aging in terms of damage mechanisms like diffused resin micro-cracking, fiber–matrix interface degradation or fiber breaking. In this effort, it is important to be able to identify quantified forms of these damage mechanisms and associated morphologies that also manifest in lower scales, by performing experiments in the macro-scale. Therefore, it is of essence to demonstrate the ability of a methodology to identify lower-scale entities such as the potentially degraded elastic properties of the interface between fibers and matrix.

The progress in the areas of computers and information in engineering and in mechatronic automation has enabled us to pursue the research areas of multi-axial robotic testing and design optimization for the purpose of data-driven constitutive characterization of anisotropic material systems. Although our efforts began three decades ago, here we present our progress, as it relates to the multi-scale inversion described above. This methodology is motivated by the data-driven requirements of employing design optimization principles for determining the constitutive behavior of composite materials as described in our recent work [MIC 11a, MIC 11c]

Traditionally, the constitutive characterization of composite materials has been determined through conventional uniaxial tests, mainly aiming at the estimation of the elastic properties for simplified stress–strain states. Typically, extraction of these properties involves several uniaxial tests conducted with specimens mounted on uniaxial testing machines, where the major orthotropic axis of any given specimen is angled relative to the loading direction. In addition, specimens are designed such that a homogeneous state of strain is developed over a well-defined area, which is required for the purpose of measuring stresses and strains through the measurement of the respective reaction forces and displacements [DAN 05, CAR 02]. Consequently, the use of uniaxial testing machines imposes requirements of using multiple specimens, griping fixtures and multiple experiments without the option of studying multi-axial effects in their full range. The requirement of a homogeneous state of strain frequently imposes restrictions on the sizes and shapes of specimens to be tested. These requirements result in increased cost and time and inefficient characterization processes.

To address these issues and to extend the characterization to a multi-axial state of strain in both the linear and nonlinear regimes, multi-degree of freedom-automated mechatronic testing machines were introduced at the Naval Research Laboratory (NRL), in conjunction with energy-based inverse characterization methodologies, [MAS 92, MAS 95]. This development was the first of its kind and has continued ever since [MIC 03, MIC 04, MIC 08]. Thus, our approach employs mechatronic testing, and although it enables multi-axial loading that induces inhomogeneous states of strain, it still requires multiple specimens. However, these specimens are tested in an automated manner with high testing throughput that has reached a peak rate of 28 specimens per hour.

In addition, the development of flexible full-field displacement and strain measurement methods during mechanical tests has afforded the opportunity of alternative characterization methodologies [PIE 07, COO 07, MIC 09b, ILI 13, ILI 14]. Methods such as Moire and speckle interferometry, digital image correlation (DIC) and some high-performance methods, such as the meshless random grid (MRG) method and the direct strain imaging (DSI) method, have been used mostly for elastic characterization of various materials [MIC 09b, BRU 02, SCH 03, KAJ 04, ILI 16]. The resulting measurements are used for the identification of constitutive model constants, via the solution of an appropriately formed inverse problem, using various computational techniques. In particular, not only the authors [MAS 92, MAS 95, MIC 03, MIC 04, MIC 08, MIC 09b] but also other groups [KAJ 04, MEU 98, MOL 05] have focused on developing a mixed numerical/experimental method that identifies the material's elastic and inelastic constants by minimizing an objective function formed by the difference between full-field experimental measurements and the corresponding analytical model predictions via an optimization method.

Our approaches are based mostly on energy conservation and can thus be classified according to computational cost in relation to the repetitive use of finite-element analysis (FEA) or not. It is important to clarify that digitally acquired images are processed by software [MIC 09a] that implements the meshless random grid (MRG) method [MIC 09b, AND 06, ILI 12, ILI 09a] to extract the displacement and strain field measurements as well as the boundary displacements required for material characterization. The development and use of the MRG method was motivated by the requirements of resolution, accuracy and computational efficiency that were higher than those available from other full-field methods. Reaction forces and redundant boundary displacement data are acquired from displacement and force sensors integrated with NRL's 6-degrees of freedom (6-DoF) multi-axial loader called NRL66.3 [MIC 10a]. In an effort to address the computational cost of the FEA-in-the-loop approaches, the authors have initiated a dissipated and total strain energy density determination approach that has recently been extended to a framework that is derived from the total potential energy and the energy conservation, which can be applied directly with full-field strain measurement for characterization [MAN 08, MIC 09c].

In the next section, we present a description of the 6-DoF loader, the associated loading space characteristics and the experimental campaign. The following section introduces an overview of two energy-based constitutive formalisms necessary for the characterization. The implementation details of the design optimization methodology follow along with characterization and validation results. The subsequent section presents the utilization of surrogate models for improving the computational efficiency of the optimization loop required for the constitutive characterization. The following section presents an application of the multi-scale cascaded inversion framework that enables utilization of experimental data at the macro-scale for determining properties at the micro-scale of the constituents. Finally, the chapter ends with a description of the conclusions drawn.

## 8.2. Automated multi-axial testing

NRL66.3 is a custom-designed and prototyped system that represents the third generation of 6-DoF loaders built by our group for the purpose of automating the process of multi-axial testing required for the data-driven constitutive characterization of composites. It was conceived to ensure that the material to be characterized will be exposed to a very comprehensive set of deformation states such that the richest set of strain states will develop inside this material. The system has a recursive character because its characteristic hexapod configuration is repeated six times and is described in [MIC 10a] and shown in Figure 8.2.

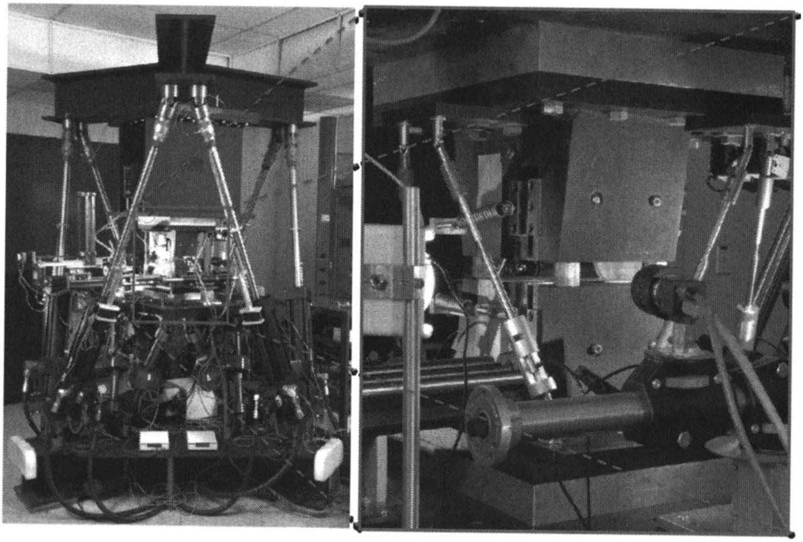

**Figure 8.2.** *NRL66.3: 6-DoF mechatronically automated system for the multi-axial testing of composite materials: long (left) and near (right) views of the system*

The typical flat specimen geometry is shown in Figure 8.3, where the dark gray areas indicate the part of the specimen that is placed into the grips and the light gray area represents the part that deforms under the influence of the applied load. The double notches on the specimen are introduced to disturb the strain field and to ensure that some areas of the specimen (not necessarily near the notch roots) will experience nonlinear constitutive response due to the corresponding strain fields. The dimensions are in "millimeters (inches)". The white dots on the deformation domain as shown in Figure 8.3 (right side) are markers required for measuring the displacement and strain field components via the MRG method [ILI 09a, ILI 09b, MIC 09a].

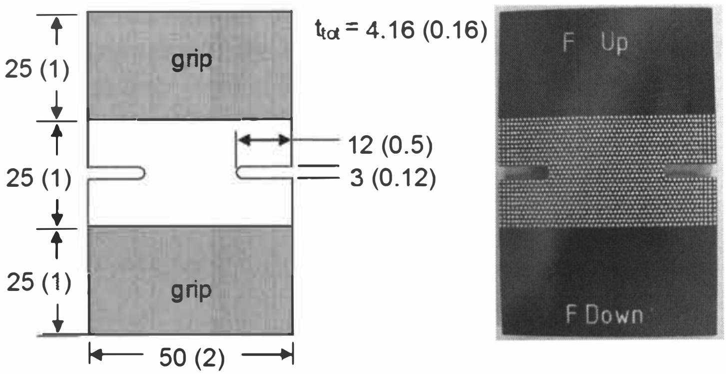


**Figure 8.3.** *Typical specimen schematic (left) and photographic view (right) of prepared specimen*

### 8.2.1. *Loading space*

Because the main mission of the system is to induce a set of strain states that is as complete as possible, it is designed such that it can be programmed to follow displacement- and rotation-controlled loading paths while it can measure boundary displacements and reaction forces and moments resulting from the mechanical response of the specimens under testing.

The hexapod configuration effectively converts the linear extension motions of the six actuators to the three translations and the three rotations imposed by the upper grip on the specimen. These three translations and three rotations effectively define a six-dimensional space that can be sampled by commanding NRL66.3 to follow radially proportional paths and acquire data along these paths. The term proportional path denotes that every path $i$, when represented as a vector starting in the origin and ending at point $j$, can be resolved to its vector space basis components in the 6-D frame $(\mathbf{u}_x, \mathbf{u}_y, \mathbf{u}_z, \mathbf{r}_x, \mathbf{r}_y, \mathbf{r}_z)$ according to:

$$\mathbf{p}_i^j = p_{i1}^j \mathbf{u}_x + p_{i2}^j \mathbf{u}_y + p_{i3}^j \mathbf{u}_z + p_{i4}^j \mathbf{r}_x + p_{i5}^j \mathbf{r}_y + p_{i6}^j \mathbf{r}_z, \qquad [8.1]$$

where $p^j_{i1}, p^j_{i2}, p^j_{i3}, p^j_{i4}, p^j_{i5}, p^j_{i6}$ are the magnitudes of each component, and furthermore:

$$p^j_{ik} = r^j_i a^j_{ik}, k \in \{1,2,3,4,5,6\}, \text{ with } a^j_{ik} = a^{j+1}_{ik}. \qquad [8.2]$$

A convenient parameterization of the loading paths can be obtained by invoking a transformation from the hyperspherical to its Cartesian frame of reference as follows:

$$\left.\begin{array}{l} p^j_{i1} = r^j_i \cos(\phi^i_1) \\ p^j_{ik} = r^j_i \cos(\phi^i_{k-1}) \prod_{m=1}^{k-1} \sin(\phi^i_m) \text{ for } k = 2, ..., 6 \end{array}\right\}, \qquad [8.3]$$

where $r^j_i$ and $\phi^j_k$ are the magnitude of the path and the angles between it and the planes defined by the basis vectors of the 6-D kinematic space.

At least as many specimens as the number of paths were used to sample the material system (material coupon) excitation space (i.e. the loading space).

The number of paths as a function of the dimension $n$ of the space and the number of equatorial points $n_{ep}$ is given by [MIC 08]:

$$n_{paths} = (4 + 4n_{ep})(1 + 2n_{ep})^{n-2}. \qquad [8.4]$$

An intermediate scenario (in terms of required number of specimens) could be based on the fact that the rotation components generate motion on the plane they are normal to. Thus, only four out of the six components can be linearly independent. In this case, $n = 4$ and for $n_{ep} = 1$, equation [8.4] generates 72 paths. This promotes the solution of utilizing one of the fifteen 4-D sub-spaces that can be used for defining the loading paths.

A computationally intensive methodology for determining the best sub-space is presented in detail elsewhere [ILI 10]. An appropriate metric representation with respect to strain state volumetric histograms was developed, and the notion of strain-state clouds (SSCs) [ILI 10] was introduced as a means of visualizing these histograms. Extensive numerical experiments were conducted on the basis of FEA computations of the elastic response of a composite specimen with edge notches. They were used as the means for generating all possible strain states generated by loading paths in the corresponding sub-spaces. A typical example of the relevant SSCs is depicted in Figs.8.4a, 8.4b for loading case 02 $(u_y, r_x, r_y, r_z)$. The color scale from blue to red indicates the distance from $\{0, 0, 0\}$ and is only used as a visual aid assisting qualitative comparison.

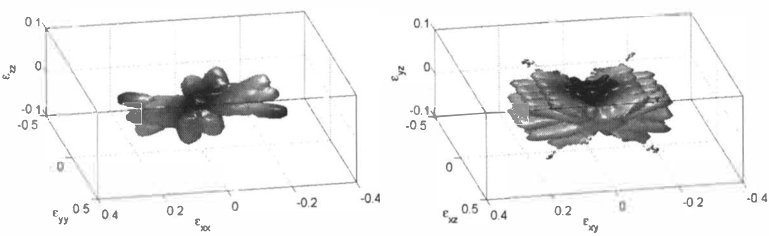

(a) Normal for L.C. 2 $(u_y, r_x, r_y, r_z)$ (b) Shear for L.C. 2 $(u_y, r_x, r_y, r_z)$

**Figure 8.4.** *Normal and Shear Strain State Clouds for a specimen with stacking sequence* $[-30°, 30°]_{16}$. *For a color version of the figure, see www.iste.co.uk/brancherie/microstructure.zip*

The ratio of the volume of each SSC to the sum of the volumes of all SSCs created by all possible loading paths within all sub-spaces was used as the load sub-space ranking metric. It was established that the sub-spaces involving all three rotations and one of the two in-plane translations generate the richest strain state sets. Here, the term "richest" signifies that the 4-D sub-spaces contain the largest sets of strain states that also appear in the full 6-D dimensional space. On the basis of an energy loss criterion, the final sub-space selected was that involving the three rotations and the tension–compression loading case.

### 8.2.2. *Experimental campaign*

The lowest number of specimens used on the basis of economical considerations was determined using a single specimen per loading path. For reasons of simple redundancy, we decided to repeat each path, and therefore each load path was followed twice by testing two specimens of identical material systems. Thus, 144 specimens per material system are required. Each material system was defined to be a balanced laminate with an alternating angle of fiber inclination per ply relative to the vertical axis of the specimen that is perpendicular to the axis defined by the two notches of the specimen. Four angles were used, $+/-\ 15, +/-\ 30, +/-\ 60, +/-\ 75$ degrees, and therefore $4 \times 144 = 576$ specimens were manufactured. The actual material used to make the specimens was an AS4/3501-6 carbon fiber/epoxy resin system.

However, because we needed to study ply thickness length scale effects, we manufactured an equal amount of specimens, where the cross-plied unidirectional laminas were made with four plies each, thus leading to thicker uniaxial laminas. This doubled the number of total specimens to 1,152, and this was the final number of required tests. All specimens were tested using NRL66.3 in May 2011. A very small sample of the testing process is shown in a video which can be found at URL http://www.youtube.com/watch?v=Cpl8y3HAqsM. On May 13, 2011, the system achieved a throughput of 20 tests/h for a total of 132 tests. On May 27, the system achieved a throughput of 25 tests/h for a total of 216 tests. On June 15, 2011, the system reached its peak throughput of 28 tests/h. All 1,152 tests were completed in 12 working days. The test yielded 13 TB of data from the sensors and the cameras of the system.

## 8.3. Constitutive formalisms

To derive the mathematical constitutive form of an anisotropic material, we adopted a modified anisotropic strain energy density function as an additive decomposition of both an elastic and an inelastic (which accounts for damage) part. However, certain classes of composite materials reach failure after small strains and some under large strains. For this reason, we adopted two cases, one involving a small (infinitesimal) strain formulation (SSF) and another involving a finite (large) strain formulation (FSF).

### 8.3.1. *Small strain formulation*

For the SSF, we introduce a strain energy density (SED) function that, in its most general form, can be represented as a scaled Taylor expansion of the Helmholtz free energy of a deformable body, which is in terms of small strain invariants of the form [MIC 14]:

$$U_{SSF}(I_n) = s_0 + s_{11}I_1 + \frac{1}{2}s_{12}I_1^2 + \frac{1}{3!}s_{13}I_1^3 + \frac{1}{4!}s_{14}I_1^4 + \dots, \quad [8.5]$$

where $I_n; n = 1, 2, 3$ are the strain tensor invariants.

After an additive decomposition of the SED in terms of recoverable and irrecoverable parts, its differentiation with respect to strain components to derive the constitutive law and subsequent algebraic manipulations [MIC 14], we can derive the expression:

$$\begin{aligned} U_{SSF} &= U^R_{SSF}(S; \varepsilon_{ij}) + U^I_{SSF}(D; \varepsilon_{ij}) = \\ &= \frac{1}{2}s_{ijkl}\varepsilon_{ij}\varepsilon_{kl} - s_{ijkl}\frac{1}{e(2+p_{ij})p_{ij}q_{ij}^{p_{ij}}}\varepsilon_{ij}^{1+p_{ij}}\varepsilon_{kl}. \end{aligned} \quad [8.6]$$

Employing the Voigt [DAN 05] notation for the case of a general orthotropic material yields the constitutive relation [MIC 14]:

$$\begin{bmatrix} \sigma_{xx} \\ \sigma_{yy} \\ \sigma_{zz} \\ \sigma_{xz} \\ \sigma_{yz} \\ \sigma_{xy} \end{bmatrix} = \begin{bmatrix} \breve{s}_{xx} & s_{xy} & s_{xz} & 0 & 0 & 0 \\ s_{xy} & \breve{s}_{yy} & s_{yz} & 0 & 0 & 0 \\ s_{xz} & s_{yz} & \breve{s}_{zz} & 0 & 0 & 0 \\ 0 & 0 & 0 & \breve{s}_{xz} & 0 & 0 \\ 0 & 0 & 0 & 0 & \breve{s}_{yz} & 0 \\ 0 & 0 & 0 & 0 & 0 & \breve{s}_{xy} \end{bmatrix} \begin{bmatrix} \epsilon_{xx} \\ \epsilon_{yy} \\ \epsilon_{zz} \\ \epsilon_{xz} \\ \epsilon_{yz} \\ \epsilon_{xy} \end{bmatrix}, \quad [8.7]$$

where:

$$\breve{s}_{ij} = s_{ij}\left(1 - \bar{d}_{ij}\right) \quad [8.8]$$

and:

$$\bar{d}_{ij} = \frac{1}{e p_{ij} q_{ij}^{p_{ij}}}\varepsilon_{ij}^{1+p_{ij}}. \quad [8.9]$$

For a transversely isotropic material, the number of material parameters is $5 + 10 = 15$ for a 3-D state of strain and $4 + 8 = 12$ for a plane stress state [JU 98, MIC 14].

### 8.3.2. *Finite strain formulation*

The FSF can be written in a form expressing the volumetric versus distortional decomposition similar to the expression given by [KAL 00]:

$$U_{FSF} = (1 - d_v)W_v(J) + (1 - d_d)W_d(\bar{C}, A \otimes A, B \otimes B), \qquad [8.10]$$

with the damage parameters $d_k \in [0, 1], k \in [v, d]$ defined as:

$$d_k = d_{ka}^{\infty}\left[1 - e^{\left(-\frac{a_k(t)}{\eta_{ka}}\right)}\right], \qquad [8.11]$$

where $a_k(t) = \max\limits_{s\in[0,t]} W_k^o(s)$ is the maximum-energy component reached so far and $d_{ka}^{\infty}, \eta_{ka}$ are two pairs of parameters controlling the energy dissipation characteristics of the two components of SED. In this formulation, $J = \det \underline{F}$ is the determinant of the deformation gradient, $\bar{C} = \underline{F^T F}$ is the right Cauchy–Green (Green deformation) tensor, $A, B$ are constitutive material directions in the undeformed configuration and $A \otimes A, B \otimes B$ are microstructure structural tensors expressing fiber directions.

Under the FSF, the material characterization problem involves determining the 36 coefficients (at most) of all monomials in addition to the compressibility constant d and the four parameters used in equation [8.11]. It follows that there can potentially be a total of 41 material constants [MIC 14].

## 8.4. Meshless random grid method for experimental evaluation of strain fields

As will be clear in the following section, it is essential that the strain tensor component fields are evaluated experimentally in order to use the relevant data for the design optimization methodology described in the next section.

After assessing the flexibility, simplicity, sensitivity, accuracy and computational efficiency requirements needed for this effort, it was concluded that existing methods did not satisfy these requirements to our satisfaction. For this reason, we developed the MRG method. Detailed descriptions of the method can be found in [MIC 11b, ILI 14]. Here, we present a short overview for the sake of completeness and we urge the reader to seek more details elsewhere [ILI 14].

The MRG method is based on the meshless representation of the displacement field considering the values of the displacement on the nodes, while the strain tensor is identified by the differentiation of those displacements.

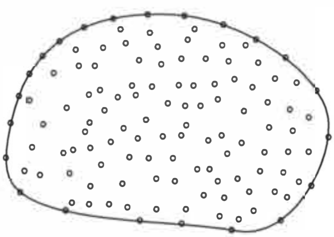

(a) Nodes in a domain

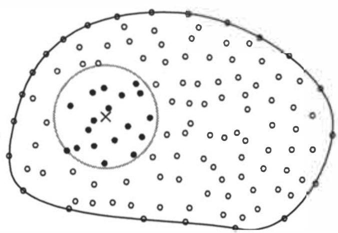

(b) A Circular domain of support for a point of interest

**Figure 8.5.** *Meshless representation*

In order to accomplish full-field measurement of strain fields, the MRG method requires a procedure involving the following four steps [ILI 07, ILI 14]:

1) A specimen is prepared by marking it with a random distribution of black dots at the area of interest.

2) Images of the non-deformed and deformed specimens are acquired, and a simple labeling algorithm is used to identify the centroids (centers of the marked dots) on each image.

3) A point-matching algorithm identifies the correspondence between centroids of the dots between the two images and calculates the respective displacement.

4) The centroid displacement values previously obtained are used to calculate the full-field values of displacement and strain through meshless functions. In the last step, there are various choices from typical meshless functions [LIU 09], including the moving least-square (MLS) method for shape function construction and point interpolation (PI) methods. In the present work, the shape function is constructed through the MLS method.

The MLS approximates the displacement field using an expression of the form:

$$u^h(\mathbf{x}) = \boldsymbol{\Phi}(\mathbf{x})\,\mathbf{U}_S, \qquad [8.12]$$

where $\mathbf{U}_S$ is a vector of displacement components of the nodes in the vicinity of the point represented by the vector $\mathbf{x}$, while:

$$\boldsymbol{\Phi}(\mathbf{x}) = [\phi_1(\mathbf{x}), \phi_2(\mathbf{x}), \ldots, \phi_n(\mathbf{x})], \qquad [8.13]$$

are shape functions calculated from expressions of the form,

$$\phi_I(\mathbf{x}) = \sum_j^m p_j(\mathbf{x}) \left[\mathbf{A}^{-1}(\mathbf{x})\,\mathbf{B}(\mathbf{x})\right]_{jI} = \mathbf{p}^T\mathbf{A}^{-1}\mathbf{B}_I, \qquad [8.14]$$

where $p_j$ represent the components of the polynomial basis $\mathbf{p}^T$ and $\mathbf{A}, \mathbf{B}_I$ are matrix compositions of the polynomial basis and appropriate weight functions. The displacement field expressed by equation [8.12] is subsequently differentiated to provide the surface strain components, fields. More details can be found in [ILI 14].

## 8.5. Inverse determination of HDM via design optimization

In order to determine the material parameters of the constitutive model that represents the behavior of the bulk lamina, the inverse problem at hand was solved through a design optimization approach described in more detail elsewhere [MIC 14]. The optimization process outline is shown in Figure 8.6.

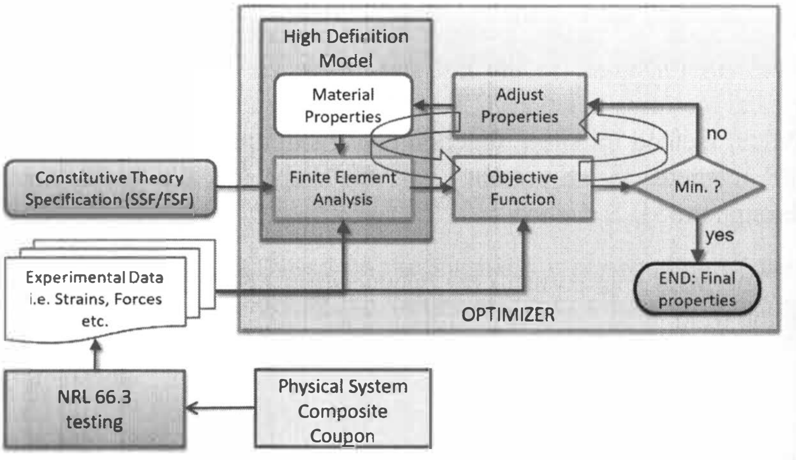


**Figure 8.6.** *Design optimization data flow for inverse characterization via utilization of HDM*

This particular scheme exercises the optimizer for the case of the high-definition model (HDM) that represents the full FEA model for the test coupon geometry. Details of this model are presented in [MIC 11c, MIC 11a] due to space limitations.

Two objective functions were constructed, and both utilized the fact that through the REMDIS-3D software [MIC 11b] developed by our group, we can obtain full-field measurements of the displacement and strain fields over any deformable body as an extension of the REMDIS-2D software that is based on the MRG method [MIC 09b, AND 06, ILI 12, ILI 09a, ILI 14, ILI 14]. Thus, our experimental measurements for the formation of the objective functions were chosen to be the strains at the nodal points of the FEM discretization. The first objective function chosen was based entirely on strains and is given by:

$$J^{\varepsilon} = \sum_{k=1}^{N} \left( \sum_{i=1}^{2} \sum_{j=i}^{2} \left( \left[ \varepsilon_{ij}^{\exp} \right]_k - \left[ \varepsilon_{ij}^{fem} \right]_k \right) \right)^2 , \qquad [8.15]$$

the second objective function is given in terms of surface strain energy density according to:

$$J^{U} \approx \oint_{\partial\Omega} \left( U^{\exp} - U^{fem} \right)^2 dS. \qquad [8.16]$$

The quantities $U^{\exp}$ and $U^{fem}$ are the surface strain energy densities formulated using the experimental strains and the FEM-produced strains, respectively. In the last two equations, the quantities $\varepsilon_{ij}^{fem}$ and $U^{fem}$ require an initial guess of the material properties as the coefficients of the respective monomials in the strain energy density function representation. Clearly, as the optimization progresses, the values of these parameters are modified until they converge to their final values.

For the case of the FSF, a two-stage optimization was performed. In the first stage, we determined the values of the coefficients of the strain invariant monomials such that the FSF matches the SSF by constructing and minimizing an objective function of the form:

$$J^{URF}(d, a_1, b_1, c_1, d_1) \approx \oint_{\partial\Omega} \left( U^{R}_{FSF} - U^{R}_{SSF} \right)^2 dS \qquad [8.17]$$

This was done in order to establish the proper parameters of the FSF model that matches the SSF model.

In the second stage, the material parameters encoding the damage behavior of the FSF were determined through the minimization of the objective function:

$$J^{UF}(d, a_1, b_1, c_1, d_1, d_a^{\infty}, \eta_a) \approx \oint_{\partial\Omega} \left( U^{1}_{FSF} - U^{2}_{FSF} \right)^2 dS \qquad [8.18]$$

where $U^1_{FSF}(\bar{d}, \bar{a}_1, \bar{b}_1, \bar{c}_1, \bar{d}_1, \bar{d}^{\infty}_a, \bar{\eta}_a)$ is the SED of the FSF for the parameters $\bar{d}, \bar{a}_1, \bar{b}_1, \bar{c}_1, \bar{d}_1$ computed from the previous step of matching the FSF model with the SSF model. The unknown constitutive model was chosen to be represented by another FSF SED, namely $U^2_{FSF}(d, a_1, b_1, c_1, d_1, d^{\infty}_a, \eta_a)$.

### 8.5.1. *Numerical results of design optimization*

For the purpose of demonstrating numerically the effectiveness of the aforementioned design optimization concepts, the material selected for generating the necessary simulated experimental data is a typical laminate constructed from a carbon fiber/epoxy resin lamina system of type AS4/3501-6. As can be evidenced by the reported values of the elastic constants for this material system by several sources [DAN 05, RYA 90, WEG 00, VAI 97] and as summarized in [MIC 14], the variability of the reported values extends from 11.1% to 78.2%. It is therefore important to identify the set of elastic material properties before and after a batch of new materials is manufactured or before a material system is used for design, material qualification or material certification.

To demonstrate the applicability of the proposed approach of solving the inverse problem for the SSF with the proposed design optimization method, we present here an example of using real data from a multi-axially loaded specimen from a test conducted by utilizing NRL66.3. The model characteristics of the specimen used are presented in Figure 8.7, in terms of both the discretization model and potential boundary conditions, and a detail in the area of the left notch shows a stacking of $[+60, -60]16$ with each lamina made out of AS4/3501-6.

By applying the outlined optimization approach for the case of the SSF, we identified the elastic constants as shown in Table 8.1, in comparison to those of [DAN 05].

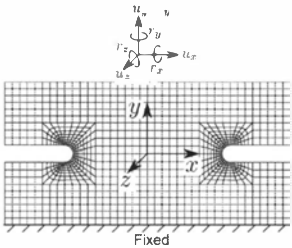


(a) Discretization and boundary conditions of typical specimen used for material characterization

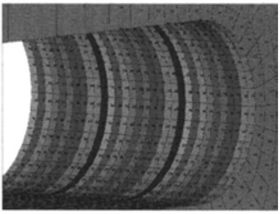

(b) Detail of FEA model near one of the notches

**Figure 8.7.** *Finite-element model*

| *Ref* | $E_{11}$ [GPa] | $E_{22}$ [GPa] | $\nu_{12}$ | $\nu_{23}$ | $G_{12}$[GPa] |
|---|---|---|---|---|---|
| Daniels [DAN 05] | 147.0 | 10.3 | 0.27 | 0.28 | 7.0 |
| Present | 125.0 | 10.8 | 0.27 | 0.32 | 7.96 |

**Table 8.1.** *Engineering properties of AS4/3501-6 laminae*

By performing FEA for the cases that correspond to the specific loading path corresponding to an experiment, we can now compare the predicted distribution of any component of the strain or stress tensor. In order to demonstrate how well the FSF formulation can capture the behavior of the characterization coupons used to obtain the data used in the characterization process, we present a typical example in terms of the distributions of $\varepsilon_{yy}$ as measured by the MRG method (left column) and as predicted by the FSF theory (right column), for both the front (top row) and the back (bottom row) in Figure 8.8.

More examples depicting comparisons between full-field measurements and model-predicted results for additional loading paths can be found in [MIC 14].

To determine the applicability of the constitutive characterization beyond the coupon geometry and length scale, additional validation tests have been performed on structures of shapes and layups different to those of the characterization coupons, to perform validation comparisons. A discussion of this activity is briefly presented in a more extended form in [MIC 12a].

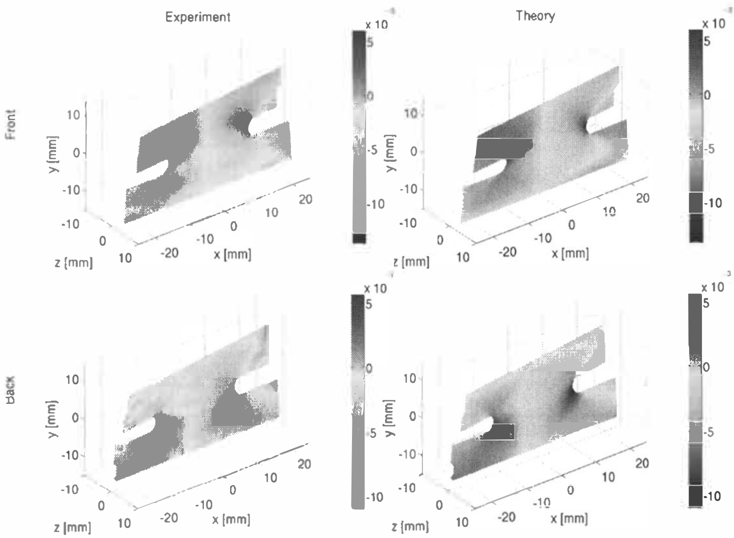


**Figure 8.8.** *Comparison of ($\varepsilon_{yy}$) field between measured (left) and the identified model using the FSF for the case of in-plane rotation and torsion of a $+/-60$ degree laminate. For a color version of the figure, see www.iste.co.uk/brancherie/microstructure.zip*

## 8.6. Surrogate models for characterization

While the previously described methodology works well from the perspective of determining the unknown material parameters, the FEA model is evaluated at every iteration of the optimization, indicating that the computational cost may be impracticable [MIC 11d]. To address this problem, we decided to explore more computationally efficient representations and methods. In particular, we investigated the replacement of the structural system model with a physics-agnostic but numerically accurate surrogate model based on non-uniform rational B-splines (NURBs) [STE 15], as illustrated in Figure 8.9. We describe here the numerical methodology for determining the proposed NURB-based surrogate models.

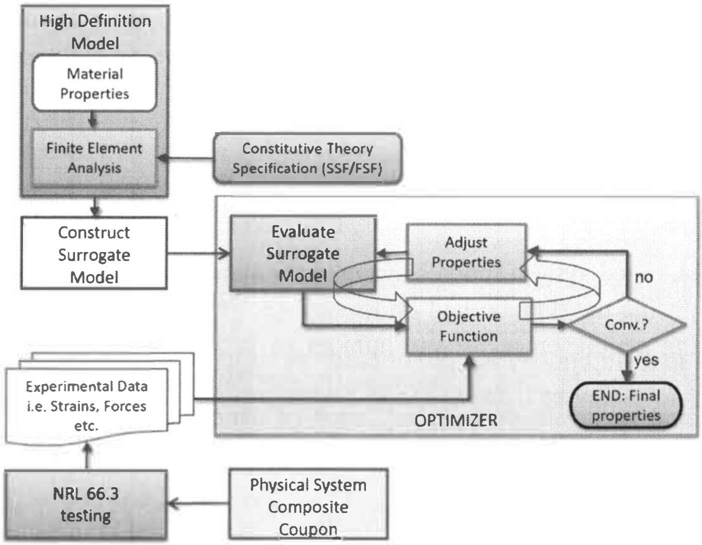


**Figure 8.9.** *Design optimization data flow for inverse characterization via utilization of a surrogate model*

In general, surrogate models are computationally efficient, but physics-agnostic representations are more expensive physics-specific models generated by sampling the underlying model and subsequently fitting some functional forms. A plethora of choices for surrogate models exists for our purposes [STE 15, TUR 05]. We used NURB-based surrogates due to the generality and computational efficiency of their formulation, as well as their established ability to represent nonlinear responses. For a particular geometry, loadings and common measurement locations and approximate solutions are sought on a system of the form:

$$\mathbf{t}^{\varepsilon}\left(\mathbf{x}_t\right) = \mathbf{c}^{\varepsilon}\left(\mathbf{a}, \mathbf{x}_c\right), \qquad [8.19]$$

where $\mathbf{t}^{\varepsilon}$ is a vector field function that collects experimentally observed strain tensor components and $\mathbf{c}^{\varepsilon}$ is a system model vector function of strain tensor components calculated by a proper method such as finite-element analysis. By introducing a surrogate model, $\mathbf{m}^{\varepsilon}$ of the original strain response model $\mathbf{c}^{\varepsilon}$ that involves the original constitutive model can be determined by equation [8.19] as:

$$\mathbf{m}^{\varepsilon}\left(\bar{\mathbf{a}}, \mathbf{x}\right) \approxeq \mathbf{t}^{\varepsilon}\left(\mathbf{x}\right) \qquad [8.20]$$

### 8.6.1. *Definition and construction of the surrogate model*

FEA-based system models evaluate the state variables onto a set of nodes inside the domain and on its surface. Thus, we assume that our sampling occurs on a discrete number of such points represented as vectors $\mathbf{x_i}, i = 1 \ldots n_m$. Consequently, our data consist of a set of $n_m$ individual surrogate models, $\mathbf{m}_i^{\varepsilon}$, each of which approximates $\mathbf{c}^{\varepsilon}$ at a single point $i$ (on the specimen surface $S_o$) represented by a vector $\mathbf{x}_i$:

$$\mathbf{m}_i^{\varepsilon}\left(\bar{\mathbf{a}}\right) = \mathbf{m}^{\varepsilon}\left(\bar{\mathbf{a}}, \mathbf{x}_i\right), i = 1 \ldots n_m \qquad [8.21]$$

The purpose of each of these surrogates is to generate a vector defined by its components as measurable scalars defined at various points of the observable part of the material specimen that depend on the constitutive parameters. We construct these surrogates in a manner that is based on the measured surface strain tensor components:

$$\mathbf{m}_i^{\varepsilon}\left(\bar{\mathbf{a}}\right) = \left\{{}_m^i\varepsilon_{xx}, {}_m^i\varepsilon_{yy}, {}_m^i\varepsilon_{xy}\right\}^T, i = 1 \ldots n_m \qquad [8.22]$$

Similarly, we define a set of experimental observations at corresponding locations, where the individual observations $\mathbf{t}_i$ have the same form as $\mathbf{m}_i$:

$$\mathbf{t}_i = \mathbf{t}\left(\mathbf{x}_i\right) = \left\{{}_t^i\varepsilon_{xx}, {}_t^i\varepsilon_{yy}, {}_t^i\varepsilon_{xy}\right\}^T, i = 1 \ldots n_m. \qquad [8.23]$$

For each of the nodes $\mathbf{x}_i \in S_o$, the system model $\mathbf{c}$ is sampled for $l$ combinations of the constitutive parameters $\mathbf{a}_q, q = 1 \ldots l$ on a uniform lattice on the vector space of $\mathbf{a}$. This sampling gives a set of vector-valued elements $\mathbf{s}_j\left(\mathbf{a}_k\right)$ that correspond to the response of $\mathbf{c}^{\varepsilon}$ at a particular location on $S_o$.

We use a direct method to produce an exact interpolation of the acquired data to fit the NURB surrogates. In the case where $\mathbf{a}_q \in \mathbb{R}^1$

(hence, $\mathbf{a}_q = a_q$), this can be formulated as the solution to a set of simultaneous linear equations:

$$\mathbf{s}_j(a_q) = \mathbf{m}_j(u_q) = \mathbf{p}_j(u_q) = \sum_{i=1}^{n_c} {}^j\mathbf{b}_i N_{i,k}(u_q),$$

$$j = 1 \ldots n_m \text{ and } q = 1 \ldots l \qquad [8.24]$$

where $N_{i,k}(u_q)$ are the NURB basis functions and ${}^j\mathbf{b}_i$ are the unknown control point locations for the single variable case. The $j^{th}$ surrogate model $\mathbf{m}_j$ is defined as equal in value to the corresponding data set $\mathbf{s}_j$ at each of the parametric coordinate values of $u_q$. The values of $u_q$ are normalized:

$$u_q = (a_q - a_{min}) / (a_{max} - a_{min}) \qquad [8.25]$$

The system of equations defined in equation [8.24] is extended to the multivariate case via the tensor product of NURB basis functions. Once the linear system has been formed, it may be solved using any technique. At the conclusion of the fitting process, $\mathbf{m}_i^\varepsilon$ are expressed as a set of interpolating functions:

$$\{\mathbf{m}_1^\varepsilon(\bar{\mathrm{a}}), \mathbf{m}_2^\varepsilon(\bar{\mathrm{a}}), \ldots, \mathbf{m}_{n_m}^\varepsilon(\bar{\mathrm{a}})\} = \{\mathbf{p}_1(\bar{\mathrm{a}}), \mathbf{p}_2(\bar{\mathrm{a}}), \ldots, \mathbf{p}_{n_m}(\bar{\mathrm{a}})\} \qquad [8.26]$$

### 8.6.2. *Characterization by optimization*

As indicated earlier, the characterization process can be formed as an inverse problem that seeks to minimize the difference between the experimentally observed and computationally calculated strain tensor components on the surface of a specimen. This is expressed in a discrete form as:

$$\text{min.} \quad f(\bar{\mathrm{a}}) = \sum_{i=1}^{n_m} \|\mathbf{p}_i(\bar{\mathrm{a}}) - \mathbf{t}_i\| \qquad [8.27]$$

$$\text{s.t.} \quad a_{min_j} \leq \bar{a}_j \leq a_{max_j} \quad \forall \quad j \in 1 \ldots n_a$$

where $n_a$ is the number of constitutive parameters (i.e. $\bar{\mathrm{a}} \in \mathbb{R}^{n_a}$). Figure 8.10 demonstrates this algorithm in a visual fashion.

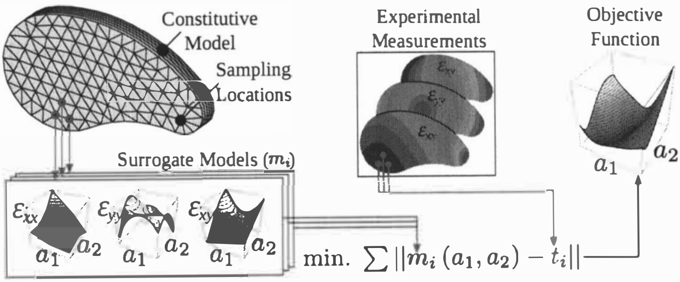


**Figure 8.10.** *Visual representation of the characterization algorithm using NURBs. For a color version of the figure, see www.iste.co.uk/brancherie/microstructure.zip*

In practice, any reasonably powerful nonlinear optimization routine can be employed. In this study, we have elected to use either simulated annealing [KIR 84] or the Nelder–Mead simplex algorithm [LAG 98], which do not require derivative information.

The presence of experimental noise complicates efforts to analyze the properties of $f$. In the formulation of equation [8.30], we now assume that the noise terms can be aggregated into a single error term $\epsilon$, which will be considered to represent a random Gaussian noise with a mean of $\boldsymbol{\mu}_\epsilon = \mathbf{0}$ and variance of $\boldsymbol{s}_\epsilon$. The law of large numbers implies that a sufficiently large $n_m$ will reduce the effect of experimental noise. The surrogate model formulation of the characterization problem can be used to combine several experimental *frames* of data, each corresponding to the same geometry, sampling locations and underlying constitutive model, but a different loading:

$$\text{min. } f(\bar{\mathbf{a}}) = \sum_{i=1}^{n_m} \left( w_1 ||\mathbf{m}^{\varepsilon}_{1,i}(\bar{\mathbf{a}}) - \mathbf{t}_{1,i}|| + w_2 ||\mathbf{m}^{\varepsilon}_{2,i}(\bar{\mathbf{a}}) - \mathbf{t}_{2,i}|| + \dots \right)$$

$$\text{s.t. } a_{min_j} \leq \bar{a}_j \leq a_{max_j} \quad \forall \quad j \in 1 \dots n_a \qquad [8.28]$$

where $w_n$ is a weight parameter associated with the $n^{th}$ load case. This approach reaps additional benefit by making $f$ more sensitive to the values of *all* of the constitutive parameters and hence avoids an ill-posed formulation [ILI 10].

| | $E_1$(GPa) | $E_2$(GPa) | $\nu_{12}$ | $\nu_{23}$ | $G_{12}$(GPa) |
|---|---|---|---|---|---|
| Recovered | 148.5 | 10.8 | 0.277 | 0.280 | 9.86 |
| Reference | 147.0 | 10.8 | 0.270 | 0.280 | 7.0 |

**Table 8.2.** *Recovery of constitutive properties from physical test data. The reference values for the parameters are taken from [DAN 05], in engineering form*

### 8.6.3. *Validation with physical experiments*

An experimental campaign was carried out using the automated test system NRL66.3 [MIC 11d] to characterize a series of AS4/3501-6 specimens. From this test campaign, 20 frames of data were chosen, one per specimen. The frames were taken from the load-path history of each experiment at a point where linear-orthotropic responses were dominant. The constitutive model used for characterization was implemented in the ANSYS FEA code. The results achieved from this process are shown in Table 6.

These results indicate that the surrogate model-based characterization can indeed be used to recover the anisotropic elastic properties of a composite from actual experimental data under real conditions. For this validation exercise, surrogate model construction required 1,015,600 s, and solving the optimization problem required 120 s. In a previous work [MIC 11d], we found that the optimization required 104,400 s. The break-even point, where the surrogate model approach yields a net improvement in computing time, thus requires only 10 experiments. Given that the campaigns associated with [MIC 11d] tested more than a thousand specimens, this is strong evidence that the surrogate-enabled methodology has practical value.

## 8.7. Multi-scale inversion

In order to achieve the inverse characterization of the composite material in multiple scales, we begin by modeling a representative volume element (RVE) of the composite structure at the micro-scale, aiming to estimate the average properties of the heterogeneous media in the meso-scale (lamina). Consequently, we have to first face the forward problem of calculating the homogenized properties of the given composite material, which, for the case of this chapter, we assume is composed of parallel, cylindrical fibers, embedded in a polymer matrix and exhibiting a periodic microstructure in either a square or hexagonal array.

Subsequently, the properties estimated by the aforementioned homogenization process are considered as the properties of the lamina at the meso-scale, which in turn forms an unsymmetric, balanced, angle-plied laminate at the macro-scale. Synthetic experiments performed on the laminate include six-axis mechanical loading, and they provide information regarding the developing strain fields. Solving the inverse structural problem involving the estimation of the composite material properties of the constituents at the micro-scale, by considering the homogenized response of the lamina in the meso-scale and the laminate in the macro-scale using experimental data collected at the macro-scale, through the use of appropriate optimization algorithms, enables the multi-scale inverse characterization of the composite material.

### 8.7.1. *Forward problem: mathematical homogenization*

Here, we focus on the three-dimensional modeling of the composite microstructure and utilize a micromechanics model that allows for the estimation of the full set of the elastic properties using a single model, as opposed to a collection of models accompanied by different assumptions in order to estimate the full set of the properties needed.

The problem of determining the material properties of heterogeneous materials, such as composites, has long been studied [ESH 57, HIL 65, BUD 65] with many analytical techniques of homogenization built upon the equivalent eigenstrain method [ESH 57], which investigates the problem of an ellipsoidal inclusion embedded in an infinite elastic medium.

The analytical methods mentioned so far provide approximate estimates of the average elastic properties of the macroscopically isotropic and sometimes anisotropic heterogeneous material. However, in order to comply with the transversely isotropic behavior that most composites exhibit due to the random distribution of fibers in the cross-section, an appropriate averaging procedure is used to provide a stiffness tensor with only five independent constants.

The current implementation involves only numerical homogenization [BAR 08] using finite-element analysis, in order to work toward the inverse problem of composite characterization at the micro-scale of constituents (fiber and matrix) in a manner that follows the established methodologies, as described in [BAR 13, YUA 08]. The composite is assumed to be composed of parallel cylindrical transversely isotropic fibers embedded in a polymer isotropic matrix. The microstructure is considered to be periodic and in either a square or a hexagonal arrangement, as shown in Figure 8.11. In order to estimate the effective elastic properties at the meso-scale, the composite is represented at the micro-scale by a 3D representative volume element (RVE), which exemplifies the arrangement of the constituents and is subjected to periodic boundary conditions [BAR 08].

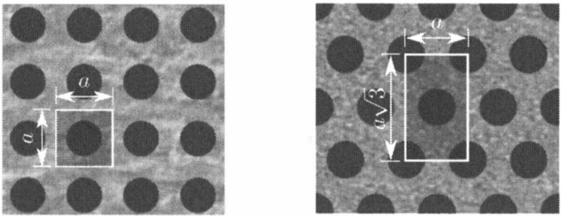


(a) Square arrangement (b) Hex arrangement

**Figure 8.11.** *Typical arrangements assumed in the homogenization of polymer matrix fiber-reinforced composite systems. Homogenization volume elements are shown in transparent red. For a color version of the figure, see www.iste.co.uk/brancherie/microstructure.zip*

Each RVE is subjected to an average strain $\bar{\epsilon}$ [LUC 98] and each of the six components of strain are applied by enforcing appropriate displacement boundary conditions through constraint equations at the faces, edges and vertices of the RVE [BAR 13]. The volume average of the strain ($\bar{\epsilon}_{ij}$) is equal to the applied strain ($\epsilon_{ij}^{app}$):

$$\bar{\epsilon}_{ij} = \frac{1}{V}\int_V \epsilon_{ij} dV = \epsilon_{ij}^{app}. \qquad [8.29]$$

For the homogeneous composite, the average stress is calculated by (in Voigt notation):

$$\bar{\sigma}_\alpha = C_{\alpha\beta}\bar{\epsilon}_\beta. \qquad [8.30]$$

Consequently, the components of the Hooke tensor $C_{\alpha\beta}$ of the homogenized material can be determined by:

$$C_{\alpha\beta} = \bar{\sigma}_\alpha = \frac{1}{V}\int_V \sigma_\alpha\left(x, y, z\right) dV \text{ , with } \epsilon_\beta^{app} = 1, \qquad [8.31]$$

where $x, y, z$ are the spatial coordinates. A detailed description of the process alongside the necessary constraint equations that satisfy periodicity for each loading case can be found in [BAR 13].

The components of $C_{ij}$ for the case of transverse isotropy are given by [DAN 05, BAR 08, KOM 15].

### 8.7.2. *Inverse problem*

As indicated earlier, like in the single-scale characterization framework [MIC 12b, MIC 12a, STE 13], the inverse problem takes the form of an optimization problem. The main difference is the fact that the forward evaluation is applied through a composed form of the models through the various scales such that the use of the experimental measurements at the macro-scale is permissible.

The constituents of the micro-scale are considered to be the matrix, the fiber and the interface between the matrix and the fiber. We assume isotropic material properties of the matrix and the interface and transversely isotropic material properties for the fiber. The properties in consideration are then defined as: $E_m$, $\nu_m$, Young's modulus and

Poisson's ratio of the matrix, respectively; $E_i$, $\nu_i$, Young's modulus and Poisson's ratio of the interface, respectively, and $E_{xf}$, $E_{yf}$, $G_{xyf}$, $\nu_{xyf}$, $\nu_{yzf}$, the five independent engineering properties of the fiber. The set of properties is denoted as:

$$P = \{E_m, \nu_m, E_i, \nu_i, E_{xf}, E_{yf}, G_{xyf}, \nu_{xyf}, \nu_{yzf}\}. \qquad [8.32]$$

Because the aim of this study is to investigate the feasibility of identifying any subset of $P$: $U \subset P$ using an appropriate inversion scheme, we can now define the set difference $K = P \setminus U$ as the set of known properties before characterization. When needed, the values of the properties in the set $U$ can be identified through simpler experiments, for example, a tension experiment to identify the matrix $E_m$ and $\nu_m$ or the fiber axial Young's modulus, $E_{xyf}$.

It is anticipated that elements of $P$ that cannot be known *a priori* will always exist. In the specific case of an RVE with an interface layer between the fiber and the matrix, these are the properties of the interface ($E_i$, $\nu_i$) that manifest only after the composite layers have been manufactured. In addition, sometimes simple elastic material constants like $\nu_{yzf}$ cannot be determined experimentally with high confidence.

In the form described herein and with the aid of the definition of the forward problem, a block diagram of the multi-scale inverse characterization process is presented in the diagram shown in Figure 8.12. The entire process is inside an optimization loop that takes the homogenized parameters and performs yet another forward evaluation of the meso- and macro-scale models. This process is performed for each load case that full-field experimental data exist for. The strain results of the multi-scale forward analysis are then incorporated into an additive operation of objective functions. These objective functions are selected to be of the form:

$$f_k = \frac{1}{3N} \sum_{l=1}^{N} \sum_{i=x,y} \sum_{j=i,y} \left| \left[\epsilon_{ij}^{exp_k}\right]_l - \left[\epsilon_{ij}^{fea_k}\right]_l \right|, \qquad [8.33]$$

where $|\cdot|$ denotes the absolute value, $\epsilon_{ij}^{exp_k}$ are the surface strains measured at pre-determined locations via any full-field measurement method in general [SEV 81, BRU 89, SIR 91, AND 05] and with the MRG or DSI methods in particular [ILI 08, MIC 09a, ILI 12, MIC 11e, ILI 11, ILI 13] for the load case $k$, $\epsilon_{ij}^{fea_k}$ are the surface strains calculated from the forward finite-element analysis of the load case $k$, $l$ is the id number of the location of the strain measurement and $N$ is the total number of strain measurement locations. An aggregate objective function $f = 1/K \sum_{k=1}^{K} f_k$ is used to collect the values of each of the objective functions evaluated for the specific load cases.

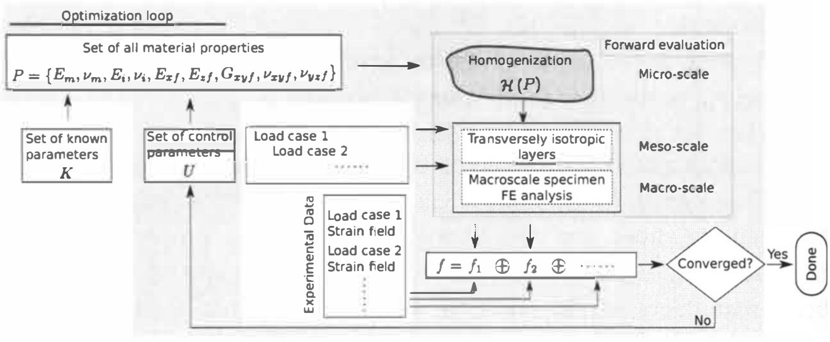


**Figure 8.12.** *Block diagram of the multi-scale inverse characterization process.*

## 8.8. Computational framework and synthetic experiments

The inverse methodology described in the previous section was implemented using MATLAB®[1] as the control language and ANSYS®Mechanical™[2] as the forward multi-scale evaluator. The connection between the two was achieved through an appropriate serial approach using file-system-based exchange of information.

1 MATLAB® is a registered trademark of The MathWorks, Inc.

2 ANSYS is a registered trademark of ANSYS, Inc.

Many optimization algorithms were explored as described in [KOM 15]. The one selected was a nonlinear derivative-free global optimization algorithm with proper modifications to constrain the search space of the optimization parameters [KOM 15].

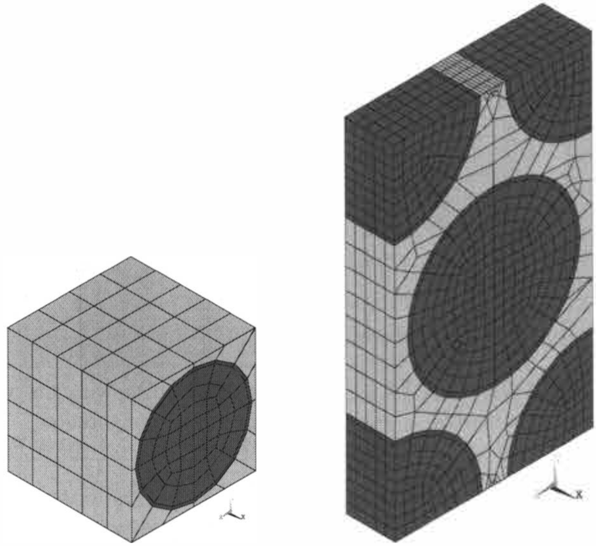

(a) Square (b) Hex

**Figure 8.13.** *Meshed unit cell geometries for a fiber-to-cell volume ratio of 0.63. Cyan: matrix; purple: fiber; red: interface layer. For a color version of the figure, see www.iste.co.uk/brancherie/microstructure.zip*

Figure 8.13 shows both the square and the hex cells utilized when an interface layer is present between the resin and the fiber.

The macro-scale geometry is presented in Figure 8.14(a). It has been discretized with hexahedral elements (SOLID185). A closeup view at the area of the hole is depicted in Figure 8.14(b). As it can be seen, the composite material layers are modeled with a single element through their thickness.

In order to investigate the capabilities of the presented multi-scale inverse method for characterizing a composite material at the constituents level by using data at the laminate level, we evaluated how accurately the elastic properties of the isotropic matrix and those of the transversely isotropic fiber can be estimated. This estimation was based on comparisons made relative to the synthetic data that were generated by running the forward problem with known constituent properties.

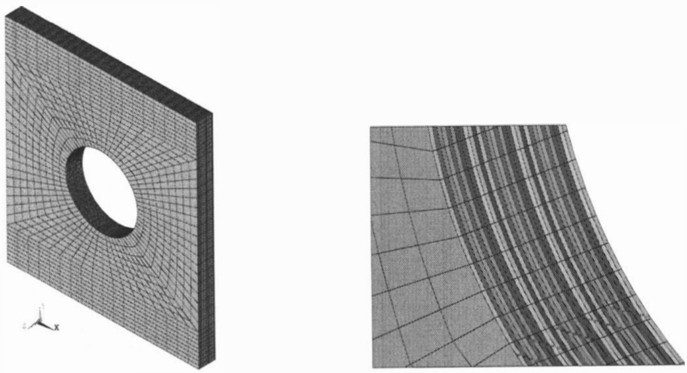

(a) General view of the meshed macro-scale specimen

(b) Close up showing the meso-scale layer configuration

**Figure 8.14.** *Meshed specimen geometry with an open hole. For a color version of the figure, see www.iste.co.uk/brancherie/microstructure.zip*

All 128 possible combinations of properties appearing in equation [8.32] were examined assuming that the interface properties $(E_i, \nu_i)$ are always unknown. With regard to the macro-scale model, the laminate specimen dimensions were chosen to be: height, 45 $mm$; width, 40 $mm$; thickness, 3.5 $mm$ and hole diameter, 15 $mm$. For all the synthetic experiments, a single loading case was selected, defined in the full loading space of a 6 degrees-of-freedom loading vector acting upon the laminate at macro-scale [ILI 10]. The values of the components of this vector for the three force components and the three components of moment were: $F_x = 2241\ N$, $F_y = 4310\ N$, $F_z = 517\ N$, $M_x = 3.45\ Nm$, $M_y = 6.9\ Nm$ and $M_z = 69\ Nm$. The magnitude of these loads was chosen to ensure that the developed corresponding levels of strain respect the linear elastic limits of the material model.

| | $E_m$ | $\nu_m$ | $E_{xf}$ | $E_{yf}$ | |
|---|---|---|---|---|---|
| Value | $4.3GPa$ | 0.35 | $235GPa$ | $15GPa$ | |
| min | $0.5GPa$ | 0.0 | $10GPa$ | $1GPa$ | |
| max | $15.0GPa$ | 0.45 | $600GPa$ | $60GPa$ | |
| | $\nu_{xyf}$ | $\nu_{yzf}$ | $G_{xyf}$ | $E_i$ | $\nu_i$ |
| Value | 0.2 | 0.07 | $27GPa$ | $2.3GPa$ | 0.25 |
| min | 0.0 | 0.0 | $1GPa$ | $0.1GPa$ | 0.0 |
| max | 0.45 | 0.45 | $75GPa$ | $5GPa$ | 0.45 |

**Table 8.3.** *Constituents material properties and optimization bounds*

The composite material used to generate the synthetic results is the AS4/3501-6 carbon epoxy, with values of elastic properties of the fiber, the matrix and the lamina as they appear in [DAN 05] and also presented in Table 8.3, together with assumed properties for the interface layer. The error for each material property reported in the relevant tables were calculated using the formula:

$$e = \left| \frac{P_{inverse} - P_{nominal}}{P_{nominal}} \right| \times 100\,[\%] \qquad [8.34]$$

where $P_{inverse}$ is the value of the property identified by the multi-scale inverse characterization and $P_{nominal}$ is the value used to generate the synthetic data.

Starting by deploying the methodology described above and utilizing the associated computational framework for only one parameter and working our way up to the total number of unknown parameters and their possible combinations, we were able to obtain a maximum number of unknown parameters which can be concurrently defined with high accuracy. We have assumed an isotropic interface zone under the condition that the matrix and fiber properties are known.

The parameter identification was successful, even for values of the interface properties as low as 0.5 % of the matrix's elastic properties. In the absence of noise in the synthetically generated data, the estimation of the interface properties can be achieved with very low error.

| ID | $E_m$ | $\nu_m$ | $E_{xf}$ | $E_{yf}$ | $\nu_{xyf}$ | $\nu_{yzf}$ | $G_{xyf}$ | $E_i$ | $\nu_i$ | Evaluations | $f$ $(pStrain)$ |
|---|---|---|---|---|---|---|---|---|---|---|---|
| sia | - | - | - | - | - | - | - | $< 0.1\%$ | $< 0.1\%$ | 124 | 2.3 |
| sib | - | - | $< 0.1\%$ | - | - | $< 0.1\%$ | $< 0.1\%$ | $< 0.1\%$ | $< 0.1\%$ | 1346 | 2.1 |
| sic | - | 0.13% | - | $< 0.1\%$ | $< 0.1\%$ | - | $< 0.1\%$ | $< 0.1\%$ | 0.8% | 3231 | 1.7 |
| sid | 0.3% | 4.2% | - | - | - | 1.2% | 4.6% | 0.65% | 35.0% | 2605 | 52.8 |

**Table 8.4.** *Multi-scale inverse characterization for selected cases of the square volume element with interface layer synthetic experiments. Case IDs represent different choices of unknown parameters*

In Table 8.4, we present some interesting inversion results for the case of the square with interface RVE. In this table, we observe that the interface properties can be found with high accuracy if the properties of the other constituents are known, which may indeed reflect a realistic situation when constituent properties can be determined experimentally. The same is true for other cases like the *sib* case. As the number of unknowns increases, the results get worse. The analysis of all 128 cases revealed that no case with more than six unknowns was inverted efficiently.

| ID | $E_m$ | $\nu_m$ | $E_{xf}$ | $E_{yf}$ | $\nu_{xyf}$ | $\nu_{yzf}$ | $G_{xyf}$ | $E_i$ | $\nu_i$ | Evaluations | $f$ $(pStrain)$ |
|---|---|---|---|---|---|---|---|---|---|---|---|
| hia | - | - | - | - | - | - | - | $< 0.1\%$ | $< 0.1\%$ | 139 | 2.0 |
| hib | - | - | $< 1.3\%$ | - | - | 19% | 10.4% | 4.2% | 52% | 485 | 509910 |
| hic | - | 1.2% | - | $< 0.1\%$ | 1.6% | - | 0.6% | 0.1% | 6.3% | 1430 | 2.1 |
| hid | 2.2% | 7.1% | - | - | - | 8.1% | 4.6% | 2.4% | 35.4% | 1485 | 347679 |

**Table 8.5.** *Multi-scale inverse characterization for selected cases of the hex volume element with interface-layer synthetic experiments*

The results of the hex RVE with interface layer are presented in Table 8.5. It is observed that in this case, the interface properties are identified when they are the only unknowns. For other cases, the properties cannot be identified with adequate accuracy, besides the *hic* case. It should be noted that this is only a subset of interesting results and that other cases have been solved with high accuracy.

## 8.9. Conclusions and plans

In this chapter, we presented a methodological framework along with its computational implementation which can be used to identify both macro- and lower-scale properties of composite materials from experiments conducted on higher scales. The macro-scale applications included both finite and infinitesimal strain formulations. In addition, its extension to use NURB-based surrogate models was presented and validated with respect to synthetic and actual experiments for the macro-scale constitutive characterization of composites.

By replacing the expensive constitutive model with an efficient surrogate in the optimization loop which drives the characterization process, material properties can be recovered in seconds, as opposed to the previously required hours or days. We have also shown that the expense of building the surrogate models is a one-time expense and that a single surrogate model can be used to characterize several material systems. In addition, we have demonstrated that the NURB-based surrogates offer a convenient method for data fusion and allow the results from many experiments to be combined in order to achieve characterization. Finally, we have demonstrated that this algorithm meets our expectations of accuracy in the presence of experimental noise and can also properly characterize physical specimens using data acquired during a robotic test campaign. We believe that their strength prompts further investigation into techniques for material characterization enabled by surrogate models.

We demonstrated the feasibility of identifying mechanical properties of constituents of composite materials at the micro-scale from experiments conducted at the macro-scale. The most interesting case is the identification of the properties of constituents that manifest only after the medium has been manufactured and could not be known *a priori* or through experimentation. We investigated the inversion methodology on the identification of properties of the interface layer that develops between the matrix and the fibers of a polymer matrix fiber-reinforced composite system. Both Young's modulus and Poisson's ratio were identified for the synthetic experiments conducted. Furthermore, it was also shown that it is possible to identify properties of other constituents as long as some of them are known.

In the future, we will conduct a sensitivity analysis with respect to the constituent material properties as well as investigate additional geometrical parameters as measures of damage mechanism evolution and incorporate the uncertainty of realistic (random) fiber distributions to eliminate the assumptions of periodic fiber arrays. We will also apply the proposed methodology by utilizing various global optimization methodologies in an attempt to establish a more detailed and efficient implementation of the inversion problem.

## 8.10. Acknowledgments

The authors acknowledge support for this study from the Office of Naval Research (ONR) through the Naval Research Laboratory's core funding. Constructive suggestions by Dr. Nathan Bechle, Forest Products Laboratory in Madison Wisconsin, are greatly appreciated.

## 8.11. Bibliography

[AND 05] ANDRIANOPOULOS N.P., ILIOPOULOS A., "Strain measurements by a hybrid experimental-numerical method using a mesh-free field function", *Honorary Volume for Professor P. S. Theocaris*, pp. 31–41, Armenian Academy of Sciences, Yerevan, 2005.

[AND 06] ANDRIANOPOULOS N.P., ILIOPOULOS A., "Displacements measurement in irregularly bounded plates using mesh free methods", *Proc. 16th European Conference of Fracture*, Alexandroupolis, Greece, 3–7 July 2006.

[BAR 08] BARBERO E.J., *Finite Element Analysis of Composite Materials*, CRC Press, Taylor & Francis Group, 2008.

[BAR 13] BARBERO E.J., *Finite Element Analysis of Composite Materials Using ANSYS*, CRC Press, Taylor & Francis Group, 2013.

[BRU 89] BRUCK H., MCNEILL S., SUTTON M. *et al.*, "Digital image correlation using Newton–Raphson method of partial differential correction", *Experimental Mechanics*, vol. 29, pp. 261–267, 1989. doi: 10.1007/BF02321405.

[BRU 02] BRUNO L., FURGIUELE F.M., PAGNOTTA L. *et al.*, "A full-field approach for the elastic characterization of anisotropic materials", *Optics and Lasers in Engineering*, vol. 37, no. 4, pp. 417–431, 2002.

[BUD 65] BUDIANSKY B., "On the elastic moduli of some heterogeneous materials", *Journal of the Mechanics and Physics of Solids*, vol. 13, pp. 223–227, 1965.

[CAR 02] CARLSSON L., ADAMS D.F., PIPES R.B., *Experimental Characterization of Advanced Composite Materials, Third Edition*, 3rd edition, CRC Press, 2002.

[COO 07] COOREMAN S., LECOMPTE D., SOL H. *et al.*, "Elasto-plastic material parameter identification by inverse methods: calculation of the sensitivity matrix", *International Journal of Solids and Structures*, vol. 44, no. 13, pp. 4329–4341, 2007.

[DAN 05] DANIEL I.M., ISHAI O., *Engineering Mechanics of Composite Materials*, 2nd edition, Oxford University Press, New York, 2005.

[ESH 57] ESHELBY J.D., "The determination of the elastic field of an ellipsoidal inclusion, and related problems", *Proceedings of the Royal Society of London A: Mathematical, Physical and Engineering Sciences*, vol. 241, no. 1226, pp. 376–396, 1957.

[FU 16] FU Y., MICHOPOULOS J.G., SONG J.-H., "On investigating the thermomechanical properties of cross-linked epoxy via molecular dynamics analysis", *Nanoscale and Microscale Thermophysical Engineering*, vol. 21, no. 1, pp. 8–25, 2016.

[HIL 65] HILL R., "A self-consistent mechanics of composite materials", *Journal of the Mechanics and Physics of Solids*, vol. 13, no. 4, pp. 213–222, 1965.

[ILI 07] ILIOPOULOS A., Digital Image Processing on Experimental Mechanics and Applications on Metallic Sheets, PhD Thesis, National Technical University of Athens, 2007.

[ILI 08] ILIOPOULOS A., ANDRIANOPOULOS N.P., "An approach to analyse errors introduced in the random grid strain measurement method", *Strain*, vol. 46, no. 3, pp. 258–266, 2008.

[ILI 09a] ILIOPOULOS A., MICHOPOULOS J., "Sensitivity analysis of the mesh-free random grid method for measuring deformation fields on composites", *Proceedings of the 17th International Conference on Composite Materials, ICCM-17, Edinburgh*, The British Composites Society: Edinburgh International Convention Centre (EICC), Edinburgh, 27–31 July 2009.

[ILI 09b] ILIOPOULOS A., MICHOPOULOS J., "Effects of anisotropy on the performance sensitivity of the mesh-free random grid method for whole field strain measurement", *ASME Conference Proceedings*, vol. 2009, no. 48999, pp. 65–74, January 2009.

[ILI 10] ILIOPOULOS A., MICHOPOULOS J., "Loading subspace selection for multidimensional characterization tests via computational experiments", *Proceedings of the ASME 2010 International Design Engineering Technical Conferences & Computers and Information in Engineering Conference IDETC/CIE 2010*, no. DETC2010/CIE-28741, ASME, 2010.

[ILI 11] ILIOPOULOS A., MICHOPOULOS J., ORIFICI A.C. *et al.*, "Experimental validation of the 2D meshless random grid method", *ASME Conference Proceedings*, vol. 2011, no. 54792, pp. 513–520, 2011.

[ILI 12] ILIOPOULOS A., MICHOPOULOS J., ANDRIANOPOULOS N.P., "Performance analysis of the mesh-free random grid method for full-field synthetic strain measurements", *Strain*, vol. 48, no. 1, pp. 1–15, 2012.

[ILI 13] ILIOPOULOS A., MICHOPOULOS J., "Direct strain tensor approximation for full field strain measurement methods", *International Journal of Numerical Methods in Engineering*, vol. 95, pp. 313–330, 2013.

[ILI 14] ILIOPOULOS A., MICHOPOULOS J., "Meshless methods for full field displacement and strain measurement", in MICHOPOULOS J.G., ROSEN D.W., PAREDIS C.J.J. *et al.* (eds), *Advances in Computers and Information in Engineering Research*, vol. 1, pp. 96–115, ASME, New York, 2014.

[ILI 16] ILIOPOULOS A., STEUBEN J.C., MICHOPOULOS J., "Determination of anisotropic mechanical properties of G-10 composite via Direct Strain Imaging", *Polymer Testing*, vol. 50, pp. 64–72, 2016.

[JU 98] JU J.W., CHABOCHE J., VOYIADJIS G.Z., *Damage Mechanics in Engineering Materials*, 1st edition, Elsevier Science, January 1998.

[KAJ 04] KAJBERG J., LINDKVIST G., "Characterisation of materials subjected to large strains by inverse modelling based on in-plane displacement fields", *International Journal of Solids and Structures*, vol. 41, no. 13, pp. 3439–3459, 2004.

[KAL 00] KALISKE M., "A formulation of elasticity and viscoelasticiy for fibre reinforced material at small and finite strains", *Computer Methods in Applied Mechanics and Engineering*, vol. 185, pp. 225–243, 2000.

[KIR 84] KIRKPATRICK S., "Optimization by simulated annealing: Quantitative studies", *Journal of statistical physics*, vol. 34, no. 5, pp. 975–986, 1984.

[KOM 15] KOMNINELLI F., ILIOPOULOS A., MICHOPOULOS J., "Towards identification of lower scale composite material properties from higher scale experimental data via inverse analysis of coupled multiscale models", *Proccedings of the ASME 2015 International Design Engineering Technical Conferences & Computers and Information in Engineering Conference*, Boston, 2–5 August 2015.

[LAG 98] LAGARIAS J.C., REEDS J.A., WRIGHT M.H. *et al.*, "Convergence properties of the Nelder–Mead simplex method in low dimensions", *SIAM Journal on optimization*, vol. 9, no. 1, pp. 112–147, 1998.

[LIU 09] LIU G.-R., *Meshfree Methods: Moving Beyond the Finite Element Method*, Taylor & Francis, Abingdon, 2009.

[LUC 98] LUCIANO R., SACCO E., "Variational methods for the homogenization of periodic heterogeneous media", *European Journal of Mechanics – A/Solids*, vol. 17, no. 4, pp. 599–617, 1998.

[MAN 08] MAN H., FURUKAWA T., KELLERMANN D., "Implicit constitutive modeling based on the energy principles", *Proceedings of XXII ICTAM*, Adelaide, 25–59 August 2008.

[MAS 92] MAST P.W., NASH G.E., MICHOPOULOS J.G. *et al.*, Experimental determination of dissipated energy density as a measure of strain-induced damage in composites, Report no. Tec. Rpt. NRL/FR/6383–92-9369, Naval Research Laboratory, Washington, DC, 1992.

[MAS 95] MAST P., NASH G., MICHOPOULOS J. *et al.*, "Characterization of strain-induced damage in composites based on the dissipated energy density. Part I. Basic scheme and formulation", *Theoretical and Applied Fracture Mechanics*, vol. 22, no. 2, pp. 71–96, 1995.

[MEU 98] MEUWISSEN M.H.H., OOMENS C.W.J., BAAIJENS F.P.T. *et al.*, "Determination of the elasto-plastic properties of aluminium using a mixed numerical-experimental method", *Journal of Materials Processing Technology*, vol. 75, nos. 1–3, pp. 204–211, 1998.

[MIC 03] MICHOPOULOS J., "Computational and mechatronic automation of multiphysics research for structural and material systems", in *Recent Advances in Composite Materials*, Kluwer Academic Press, 2003.

[MIC 04] MICHOPOULOS J., "Mechatronically automated characterization of material constitutive response", *Proceedings of the 6th World Congress on Computational Mechanics (WCCM-VI)*, Tsinghua University Press and Springer, pp. 486–491, Beijing, China, 5–10 September 2004.

[MIC 08] MICHOPOULOS J., HERMANSON J.C., FURUKAWA T., "Towards the robotic characterization of the constitutive response of composite materials", *Composite Structures*, vol. 86, nos. 1–3, pp. 154–164, 2008.

[MIC 09a] MICHOPOULOS J., ILIOPOULOS A., "A computational workbench for remote full field 2D displacement and strain measurements", *ASME Conference Proceedings*, vol. 2009, no. 48999, pp. 55–63, 2009.

[MIC 09b] MICHOPOULOS J., ILIOPOULOS A., FURUKAWA T., "Accuracy of inverse composite laminate characterization via the mesh free random grid method", *ASME Conference Proceedings*, vol. 2009, no. 48999, pp. 367–374, 2009.

[MIC 09c] MICHOPOULOS J., FURUKAWA T., LAMBRAKOS S., "Data-driven characterization of composites based on virtual deterministic and noisy multiaxial data", *2008 ASME International Design Engineering Technical Conferences and Computers and Information in Engineering Conference, DETC 2008*, vol. 3, pp. 1095–1106, New York, 2009.

[MIC 10a] MICHOPOULOS J., HERMANSON J.C., ILIOPOULOS A., "Towards a recursive hexapod for the multidimensional mechanical testing of composites", *ASME Conference Proceedings*, vol. 2010, no. 44113, pp. 91–99, ASME, 2010.

[MIC 10b] MICHOPOULOS J., LAMBRAKOS S.G., ILIOPOULOS A., "On a data and requirements driven multi-scale framework linking performance to materials", *ASME Conference Proceedings*, vol. 2010, no. 44113, pp. 197–210, ASME, 2010.

[MIC 11a] MICHOPOULOS J., HERMANSON J.C., ILIOPOULOS A. *et al.*, "Overview of constitutive response characterization for composite materials via data-driven design optimization", *Proceedings of the ASME 2011 International Design Engineering Technical Conferences & Computers and Information in Engineering Conference IDETC/CIE*, Washington, DC, 29–31 August, 2011.

[MIC 11b] MICHOPOULOS J., ILIOPOULOS A., "A computational workbench for remote full field 3D displacement and strain measurements", *Proceedings of the ASME 2011 International Design Engineering Technical Conferences & Computers and Information in Engineering Conference IDETC/CIE*, Washington, DC, 29–31 August, 2011.

[MIC 11c] MICHOPOULOS J., HERMANSON J.C., ILIOPOULOS A. *et al.*, "Data-driven design optimization for composite material characterization", *Journal of Computing and Information Science in Engineering*, vol. 11, no. 2, 2011.

[MIC 11d] MICHOPOULOS J., HERMANSON J.C., ILIOPOULOS A. *et al.*, "Data-driven design optimization for composite material characterization", *Journal of Computing and Information Science in Engineering*, vol. 11, no. 2, p. 021009, 2011.

[MIC 11e] MICHOPOULOS J., ILIOPOULOS A., "A computational workbench for remote full field 3D displacement and strain measurements", *ASME Conference Proceedings*, vol. 2011, no. 54792, pp. 489–498, ASME, 2011.

[MIC 12a] MICHOPOULOS J., HERMANSON J.C., ILIOPOULOS A., "Robotic and multiaxial testing for the constitutive characterization of composites", *Materials Challenges in Alternative & Renewable Energy*, Clearwater, FL, February 26–March 1, 2012.

[MIC 12b] MICHOPOULOS J., HERMANSON J.C., ILIOPOULOS A., "First industrial strength multi-axial robotic testing campaign for composite material characterization", *2012 ASME International Design Engineering Technical Conferences & Computers and Information in Engineering Conference*, Chicago, IL, 12–15 August, 2012.

[MIC 14] MICHOPOULOS J., HERMANSON J.C., ILIOPOULOS A., "Advances on the constitutive characterization of composites via multiaxial robotic testing and design optimization", in MICHOPOULOS J.G., ROSEN D.W., PAREDIS C.J.J. *et al.* (eds), *Advances in Computers and Information in Engineering Research*, vol. 1, ASME, New York, 2014.

[MOL 05] MOLIMARD J., LE RICHE R., VAUTRIN A. *et al.*, "Identification of the four orthotropic plate stiffnesses using a single open-hole tensile test", *Experimental Mechanics*, vol. 45, pp. 404–411, 2005. doi: 10.1007/BF02427987.

[PIE 07] PIERRON F., VERT G., BURGUETE R. *et al.*, "Identification of the orthotropic elastic stiffnesses of composites with the virtual fields method: sensitivity study and experimental validation", *Strain*, vol. 43, no. 3, pp. 250–259, 2007.

[RYA 90] RYAN K.F., "Dynamic response of graphite/epoxy plates subjected to impact loading", Thesis (M.S.), Massachusetts Institute of Technology, Dept. of Aeronautics and Astronautics, available at: http://dspace.mit.edu/handle/1721.1/42982, 1990.

[SCH 03] SCHMIDT T., TYSON J., GALANULIS K., "Full–field dynamic displacement and strain measurement using advanced 3d image correlation photogrammetry: part 1", *Experimental Techniques*, vol. 27, no. 3, pp. 47–50, 2003.

[SEV 81] SEVENHUIJSEN J., "Two simple methods for deformation demonstration and measurement", *Strain*, vol. 17, no. 1, pp. 20–24, 1981.

[SIR 91] SIRKIS J., LIM T., "Displacement and strain measurement with automated grid methods", *Experimental Mechanics*, vol. 31, pp. 382–388, 1991. doi: 10.1007/BF02325997.

[STE 13] STEUBEN J., MICHOPOULOS J., ILIOPOULOS A. *et al.*, "Inverse characterization of composite materials using surrogate models", *ASME 2013 International Design Engineering Technical Conferences & Computers and Information in Engineering Conference IDETC/CIE 2013*, no. DETC/CIE2013–12656, ASME Press, Portland, Order No.: I924DV, pp. 1–12, August 2013.

[STE 15] STEUBEN J., MICHOPOULOS J., ILIOPOULOS A., *et al.*, "Inverse characterization of composite materials via surrogate modeling", *Composite Structures*, vol. 132, pp. 694–708, 2015.

[TUR 05] TURNER C.J., CRAWFORD R.H., "Selecting an appropriate metamodel: the case for NURBs metamodels", *ASME 2005 International Design Engineering Technical Conferences and Computers and Information in Engineering Conference*, American Society of Mechanical Engineers, pp. 759–771, 2005.

[VAI 97] VAIDYA R., SUN C., "Fracture criterion for notched thin composite laminates", *AIAA Journal*, vol. 35, no. 2, pp. 311–316, 1997.

[WEG 00] WEGNER P.M., ADAMS D.F., Verification of the Combined Load Compression (CLC) Test Methods, Report no. DOT/FAA/AR-00/26, DOT/FAA, 2000.

[YUA 08] YUAN Z., FISH J., "Toward realization of computational homogenization in practice", *International Journal for Numerical Methods in Engineering*, vol. 73, no. 3, pp. 361–380, 2008.

MECHANICAL ENGINEERING AND SOLID MECHANICS SERIES

# From Microstructure Investigations to Multiscale Modeling

*Bridging the Gap*

Edited by
Delphine Brancherie
Pierre Feissel, Salima Bouvier
and Adnan Ibrahimbegović

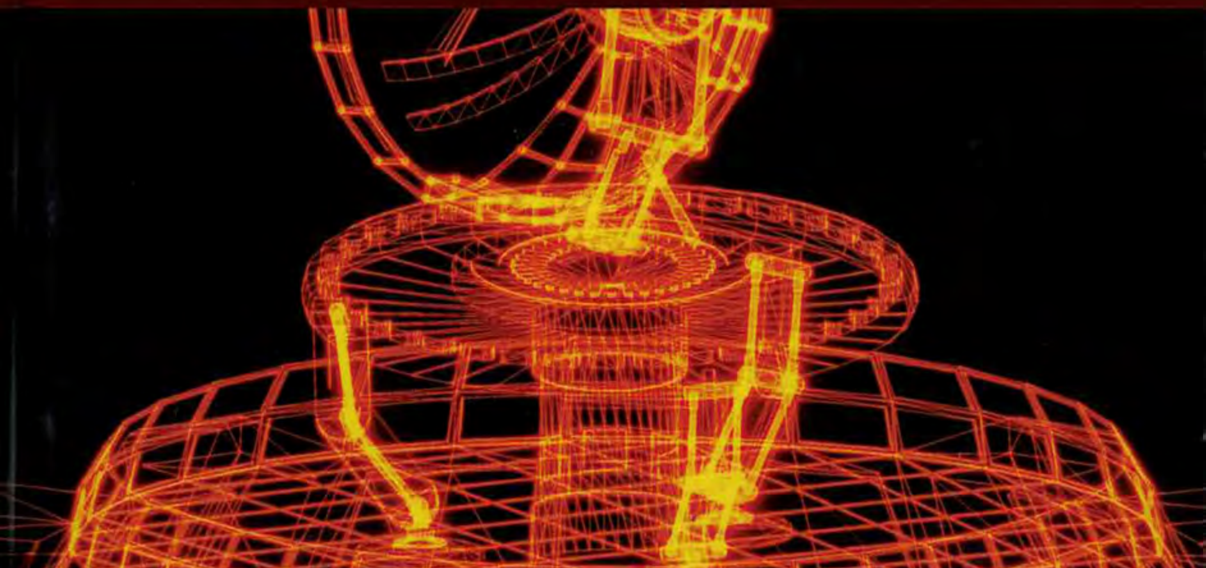

ISTE

WILEY

First published 2017 in Great Britain and the United States by ISTE Ltd and John Wiley & Sons, Inc.



ISTE Ltd
27-37 St George's Road
London SW19 4EU
UK

www.iste.co.uk

John Wiley & Sons, Inc.
111 River Street
Hoboken, NJ 07030
USA

www.wiley.com



Library of Congress Control Number: 2017953125

British Library Cataloguing-in-Publication Data
A CIP record for this book is available from the British Library
ISBN 978-1-78630-259-5

MIX
Paper from responsible sources
FSC® C013604